Measurement 132 (2019) 387–401

Contents lists available at ScienceDirect

Measurement

journal homepage: www.elsevier.com/locate/measurement

Simulation of the electric field and the GPR resulting from vertical-driven rods earthing system in a multi-layers earth structure

M. Talaat [a,b,*], M.A. Farahat [a], Mohamed A. Essa [c], M.S. Maowwad [a]

[a] Electrical Power & Machines Department, Faculty of Engineering, Zagazig University, Egypt
[b] Electrical Department, College of Engineering, Shaqra University, Dawadmi, Ar Riyadh, Saudi Arabia
[c] Mechanical Power Department, Faculty of Engineering, Zagazig University, Egypt

ARTICLE INFO

Article history:
Received 23 July 2015
Received in revised form 4 September 2018
Accepted 25 September 2018
Available online 28 September 2018

Keywords:
Earthing system
Electric field
Ground potential rise
Numerical calculation of earth potential
Finite element method
Thermal effect

ABSTRACT

A three-dimensional model for calculating the ground potential rise and the electric field distributed at the ground surface of an earthing system using driven vertical rods is presented. The electric field distribution is obtained by using Laplace's equation which is solved by finite element method. The presented model for simulating electrical field is a three-dimensional field problem with different types of earth models; one and two- layers earth models, in two different cases. The first case is represented by one driven rod while the second one is represented by three driven rods. The strength of the finite element method in this application is in its ability to allow a detailed representation of the types of the soil and different cases of the rod simulation. The new simulation model has been assessed through comparing the vertical field strength over the vertical driven rod surface, with that estimated one in other experimental and computational work. A primarily simulation for investigating the thermal effect is achieved and more investigation about this point will be presented in the future papers.

1. Introduction

Earthing systems can divert large currents safely to the earth such as lightning which has fast rise-times and can subject electrical power systems to high voltages and currents. On high voltage systems, earthing system must protect human beings from harm and minimize damage to electrical power system equipment [1,2].

Grids of grounding rods are considered an effective solution for earthing systems for all sites which must be protected from lightning strokes such as, silos, petroleum fields and telecommunication towers [3]. Vertical ground rods are the most commonly used and the simplest means for earth termination of lightning protection systems. As the more the numbers of the vertical rods increased in the grounding grid the more their performance improved [3], especially for the calculation of the ground potential rise (GPR). This is due to the reducing not only the grid resistance but also the touch and step voltage to values that are safe for humans [2–5].

The electric fields excited by the fault or lightning current are one of the most dangerous effects on the earthing system. So, the knowledge of high voltages that may be developed near earthing systems is required [6]. For such purpose, accurate evaluation of electric field at the surface of the grounding system is necessary [6–8]. The calculation of the transferred potential from the earthing system area into the outer space should also be given a special attention [8].

A proper design of an earthing system requires complete knowledge of the electric field distribution. For a simple physical system, it is usually possible to find an analytical solution. However, in many cases, the physical systems are so complex that it is extremely difficult, if not impossible, to find analytical solutions [9–13]. In such cases, numerical methods are employed for electric field calculations such as the Finite Element Method (FEM), and the Charge Simulation Method (CSM) [14–20].

The advantage of FEM over other methods is that it can consider many layers of soil, since in nature it is anisotropic resistivity, and it can be considered for different types and configurations of the earthing systems regardless of the size, length, type and shapes of the electrodes. With COMSOL Multiphysics software, knowing the soil resistivity and the dimensions of earthing systems the ground potential rise and the electric field can be obtained using the basic principle of the three dimensions of FEM.

In this paper, a mathematical model for one and three rods in one layer and two layers of earth soils which are embedded in the soil is presented, the rods. Hence, accurate computation of the electric field is a pre-requisite for determining the surface potential rise and calculating the electric field along the rod of

* Corresponding author. Tel.: +20 1005030549.
E-mail addresses: m_mtalaat@zu.edu.eg, m_mtalaat@yahoo.com (M. Talaat).

https://doi.org/10.1016/j.measurement.2018.09.067
0263-2241/

the vertical axis and the distribution of the electric field at the ground surface. The FEM is used for calculating the potential and the electric field inside the soils and in the surrounding medium. This is achieved by using COMSOL Multiphysics program.

2. Mathematical model

2.1. One layer- earth model (isotropic resistivity)

2.1.1. Single-driven rod

The potential due to any current source can be expressed as given by [12]; If the current density, J, at a top cylindrical surface with radius, r_1, considered as hemi-sphere area, and current source, I, as shown in Fig. 1, is given by

$$J = \frac{I}{2\pi r_1^2} \tag{1}$$

The electric field intensity, E, is given by

$$E = \rho J \tag{2}$$

where, ρ is the soil resistivity

$$-\nabla V = \rho \frac{I}{2\pi r_1^2} \tag{3}$$

where, $E = -\nabla V$, and V is the applied voltage to the rod,

At any point on the ground surface far with distance R, assuming that, $R \gg r_1$ and the rod represented as point with respect to this huge area as shown in Fig. 1. This point affected by the electrode electric field intensity is given by

$$\begin{aligned} -\nabla V &= \rho \tfrac{I}{2\pi R^2} \\ \therefore V &= \tfrac{\rho I}{2\pi R} \end{aligned} \tag{4}$$

The potential $\varnothing$ at any point is a function of r and z, so $R = \sqrt{r^2 + z^2}$

$$\varnothing = \frac{\rho I}{2\pi} \frac{1}{\sqrt{r^2 + z^2}} \tag{5}$$

In the isotropic resistivity, the expression of the potential satisfies Laplace's equation due to its symmetry around the cylindrical axial,

$$\nabla^2 \varnothing = 0.0$$

So, the potential is given by (see Appendix A),

$$\varnothing = \frac{\rho I}{2\pi} \int_0^\infty J_o(mr) \cos(mz) dm \tag{6}$$

$$\varnothing = \frac{\rho I}{2\pi} \int_0^\infty e^{-m|z|} J_o(mr) dm \tag{7}$$

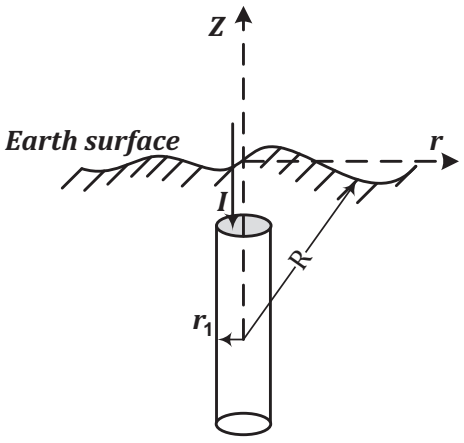

Fig. 1. Single driven rod-one layer earth model.

At the driven rod surface, the potential $\varnothing$ is to the applied voltage V of the electrode with $R = r_1$ which is very small as compared to the length l, as shown in Fig. 2(a)

$$\begin{aligned} \therefore \varnothing &= V \\ \tfrac{\rho I}{2\pi} \int_0^\infty e^{-m|z|} J_o(mr) dm &= \tfrac{\rho I}{2\pi R} \\ \therefore \int_0^\infty e^{-m|z|} J_o(mr) dm &= \tfrac{1}{R} \end{aligned} \tag{8}$$

Eq. (8) is satisfied only at the top surface of the driven electrode, where, the potential $\varnothing$ is equal to the applied voltage V, this is the first boundary condition of the FEM simulation.

At any point on the earth surface, as shown in Fig. 2a, the potential at the ground surface is given by

$$\varnothing = \frac{\rho I}{2\pi y} \tag{9}$$

where, y is the distance from the top surface of the driven electrode to the point x at the earth surface and x is the horizontal distance far from the center of the driven electrode axis.

The fictitious image of the driven rod above the ground surface is presented to maintain the potential in the center above the driven rod at a constant value [7], see Fig. 2a.

For the change of angle α from β to $-\beta$ for each of the driven rod and its image respectively, there will be a change in the length of the driven electrode with distance of dl, as shown in Fig. 2b.

From Fig. 2b,

$$\sin\alpha = \frac{y d\alpha}{dl}$$

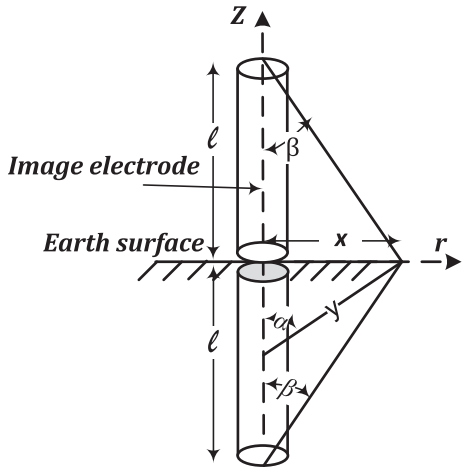

Fig. 2a. Dimensions of one driven rod and its image for one layer earth model.

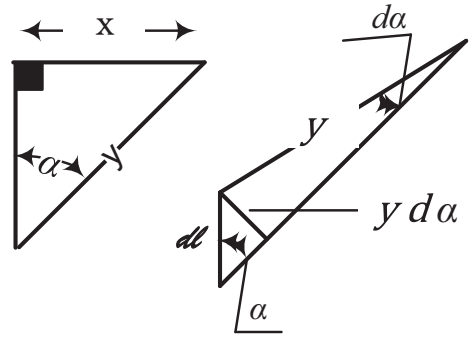

Fig. 2b. Schematic diagram of dimension and angle estimation.

where, $dl = \frac{l}{w}$ and w is the number of points on the driven electrode which is affected by the injection current [7].

$$\therefore y = \frac{\sin\alpha}{d\alpha} dl = \frac{\sin\alpha}{d\alpha}\frac{l}{w}$$

By substituting in Eq. (9), for $2w$ number of current points from β to $-\beta$ as follows,

$$d\varnothing = \frac{\rho I/(2w)}{2\pi y}$$
$$\varnothing = \frac{\rho I}{2\pi}\frac{1}{2w}\int_{\beta}^{-\beta}\frac{1}{\sin\alpha}\frac{w}{l}d\alpha$$
$$\varnothing = \frac{\rho I}{4\pi l}\int_{\beta}^{-\beta}\frac{d\alpha}{\sin\alpha} \quad (10)$$
$$\varnothing = \frac{\rho I}{4\pi l}2\left[\ln\left(\cot\frac{\beta}{2}\right)\right]$$
$$\therefore \varnothing = \frac{\rho I}{2\pi l}\ln\left(\cot\frac{\beta}{2}\right)$$

On the surface of the ground, the electric field strength can be calculated from,

$$E = \frac{d\varnothing}{dx} = \frac{d\varnothing}{d\beta}\frac{d\beta}{dx}$$

From Fig. 2a, β is correlated to x by,

$$\tan\beta = \frac{x}{l}$$

$$\frac{d\beta}{dx} = \frac{\cos^2\beta}{l}$$

and from Eq. (10),

$$\frac{d\varnothing}{d\beta} = \frac{\rho I}{2\pi l}\frac{1}{\sin\beta}$$
$$\therefore E = \frac{\rho I}{2\pi l}\frac{\cos^2\beta}{l} = \frac{\rho I}{2\pi l^2}\frac{\cos\beta}{\tan\beta} = \frac{\rho I}{2\pi l^2}\frac{\cos\beta}{x/l} \quad (11)$$
$$\therefore E = \frac{\rho I}{2\pi l}\frac{\cos\beta}{x}$$

2.1.2. The three-driven rods

From Eq. (10), for multiple driven rods which are connected in parallel, see Fig. 3, the potential at the surface of the first driven rod is given by,

$$\varnothing_1 = \frac{\rho}{2\pi l}\left[I_1 + I_2\ln\left(\cot\frac{\beta_2}{2}\right) + I_3\ln\left(\cot\frac{\beta_3}{2}\right)\right] \quad (12)$$

If the driven rods are connected by zero resistance and located symmetrically and respectively to one another, the potential and the current are as follows,

$$\varnothing_1 = \varnothing_2 = \varnothing_3 = \varnothing$$

$$I_1 = I_2 = I_3 = \frac{I}{3}$$

Therefore,

$$\varnothing = \frac{\rho}{2\pi l}\frac{I}{3}\left[1 + \ln\left(\cot\frac{\beta_2}{2}\right) + \ln\left(\cot\frac{\beta_3}{2}\right)\right] \quad (13)$$

2.2. The two layers – Earth model (anisotropic resistivity)

2.2.1. Single- driven rod

The potential due to two current sources, one in the first (upper) layer I_1, and another one in the second (lower) layer I_2 [21], see Fig. 4, can be expressed as follows,

In the non-homogenous resistivity, the expression of the potential satisfies Laplace equation due to the symmetry of the potential around the cylindrical axial,

$$\nabla^2\varnothing = 0.0$$

So, the potential at the earth surface due to the upper current source (see Appendix B), is given as follows,

$$\varnothing_1 = \varnothing_o + \int_0^{\infty} A_1(m)(e^{-mz} + e^{mz})J_o(mx)dm \quad (14)$$

The value of $A_1(m)$ can be determined using initial boundary conditions;

$$\left.\begin{array}{l}(1)\ as\ \ z\to\infty,\ \ \varnothing_1 = 0\ and\ \varnothing_2 = 0\\ (2)\ at\ \ z = 0,\ \ \partial\varnothing_1/\partial z = 0\ and\ \partial\varnothing_2/\partial z = 0\\ (3)\ at\ \ z = -h,\ \ \varnothing_1 = \varnothing_2\ and\ \frac{1}{\rho_1}\frac{\partial\varnothing_1}{\partial z} = \frac{1}{\rho_2}\frac{\partial\varnothing_2}{\partial z}\\ (4)\ at\ \ z = -t,\ \ \varnothing_2 = k\int_{-t}^{0}\frac{\partial\varnothing_1}{\partial z}dz\ where,\ k = \frac{\rho_2-\rho_1}{\rho_2+\rho_1}\end{array}\right\} \quad (15)$$

Applying these boundary conditions, the potential at the earth surface due to the upper current source is given as follows,

$$\varnothing_1 = \frac{\rho_1 I_1}{2\pi}\int_0^{\infty}\frac{e^{-mt} + ke^{-2mh}e^{mt}}{1 - ke^{-2mh}}J_o(mx)dm \quad (16)$$

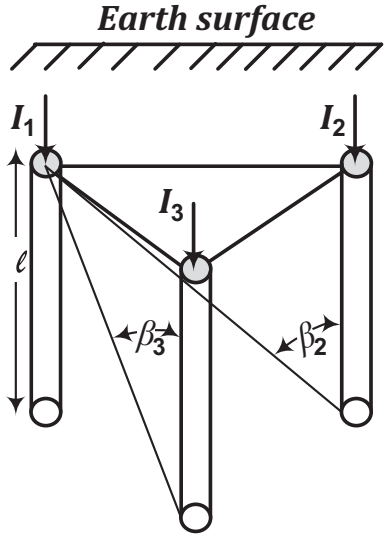

Fig. 3. Three driven rod-one layer earth model.

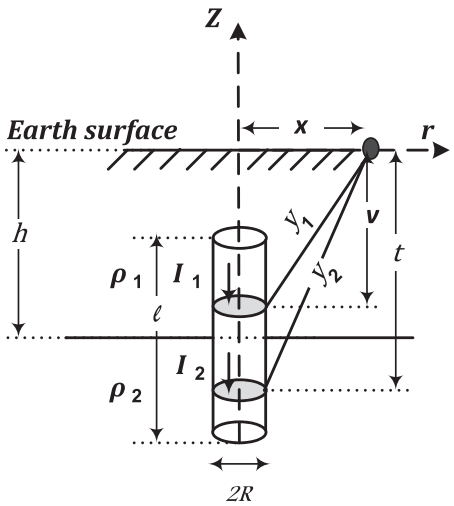

Fig. 4. Single driven rod-two layers earth model.

Similarly, the potential at the earth surface due to the lower current source is given as,

$$\varnothing_2 = \frac{\rho_2 I_2}{2\pi}\int_0^{\infty}\frac{(1-k)e^{-mt}}{1-ke^{-2mh}}J_o(mx)dm \tag{17}$$

The electric field due to the two current sources is given by

$$E_1 = -\nabla\varnothing_1 \ \ and \ \ E_2 = -\nabla\varnothing_2$$

The total potential due to the two current sources can be estimated as follows,

$$\varnothing_t = \int_{-h}^{0} E_1 dz + \int_{-(h+l/2)}^{-h} E_2 dz \tag{18}$$

The electric field due to the two current sources can be calculated as follows,

$$E = -\nabla\varnothing_t$$

2.2.2. The three- driven rods

Eq. (10), can be modified for three driven rods connected in parallel in two-layers earth model (see Fig. 5), the potential at the surface of the first driven rod is given as follows,

$$\varnothing_1 = \varnothing_{11} + \varnothing_{12} \tag{19}$$

where,

$$\varnothing_{11} = \frac{\rho_1}{2\pi l_1}\left[I_{11} + I_{21}\ln\left(\cot\frac{\beta_{21}}{2}\right) + I_{31}\ln\left(\cot\frac{\beta_{31}}{2}\right)\right]$$

$$\varnothing_{12} = \frac{\rho_2}{2\pi l_2}\left[I_{12} + I_{22}\ln\left(\cot\frac{\beta_{22}}{2}\right) + I_{32}\ln\left(\cot\frac{\beta_{32}}{2}\right)\right]$$

2.3. Earthing system resistance calculation

The value of the earthing system resistance can be calculated according to Sunde's equation [22] given by,

$$\therefore R = \frac{E}{Jlk'}\Omega \tag{20}$$

where, R, is the earthing system resistance, l is the electrode length and k' is a factor according to Sunde's equation [22].

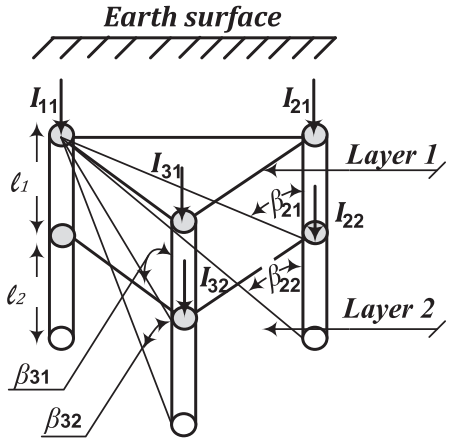

Fig. 5. Three driven rod-two layers earth model.

3. The simulation Model

This model can be simulated using the principles of FEM [23–26] for both the isotropic and anisotropic resistivity for one and three driven rods using a computer software called COMSOL Multiphysics [23,24], this gives the facility to simulate the real materials of copper rods buried in different types of soils and the same soil with different properties.

Basic cut lines are also built to study the change in the potential and the electrical field along the electrode in x, y and z axes and on the surface of earth in the zone over the place where the electrode is installed as shown in Fig. 6.

3.1. One-driven vertical rod

Fig. 7i shows the simulation of one-driven rod in one and two layers earth models. This electrode is made of copper with 2m in length, 0.2m in diameter, buried in an infinite domain of earth, but for satisfying the boundary conditions in Eq. (15), this domain can be optimized to a sample cubic of earth which has a dimension of 8m in length, 8m in width and 5.5m in height. The distance between the upper surface of the driven rod and the surface of the earth is 0.5m. The rod is subjected to an applied voltage which is expressed as per-unit,$V = 1p.u.$, while the results of per-unit do not change by different applied voltage.

3.2. The three-driven vertical rods

Fig. 7ii shows three driven vertical rods of copper in one and two layers earth models with a dimension of2m in length, 0.2m in diameter, 2m apart from each one forming a positions of triangle shape and connected together with three bars of copper, buried in sample cubic of earth which has a dimension of 8min length, 8min width and 5.5m in height and the distance between the top of the rods to the surface of the earth is 0.5m. The voltage applied for one rod (energized driven electrode) is $V = 1p.u.$

3.3. Mesh statics and analysis condition of FEM results

Numerical calculations were performed using partial differential equations (PDE) solutions [27–31]. In general, a three-dimensional (3D) problem space, using Comsol Multiphysics program [23], is divided into triangular elements (see Table 1), and the variables are approximated by the second or the third order polynomials in each element with a maximum element size equal 0.8, minimum element size equal 0.144 and the rate of growth of maximum element is 1.5, as shown in Fig. 7iii.

3.4. The soil resistivity for two-layer earth model

Soil resistivity is determined by the soil depth, type, and the soil stratification [32]. The most commonly used models for the simulation of the soil resistivity are the one and two layers soil models, while the two layers soil models often a good approximation of many and real soil structures (see Table 2), for different soil resistivity. In this paper two selected resistivity are used, clay and sand.

The electric potential satisfies Laplace's equation, with the following boundary conditions for isotropic resistivity (one-layer earth model), on the top surface of the driven electrodes $\varnothing = V$, otherwise, $\varnothing$ is calculated using Eq. (10) therefore, Laplace's equation satisfies in any regions adjacent to the driven

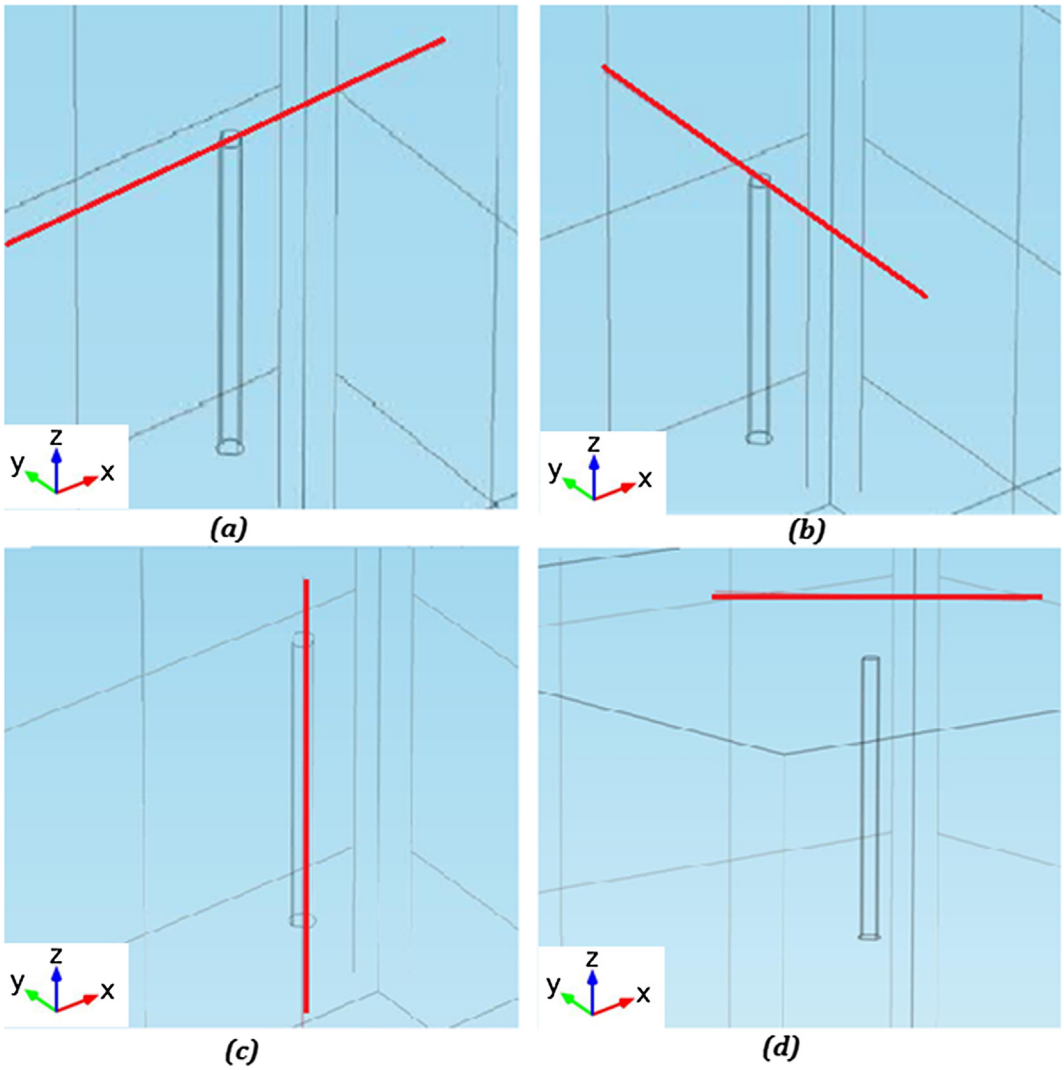

Fig. 6. The basic cut line of the potential along: (a) the electrode surface in x-axis, (b) the electrode surface in y-axis, (c) the central axis of the electrode in z-axis and (d) the earth potential surface above the driven electrode.

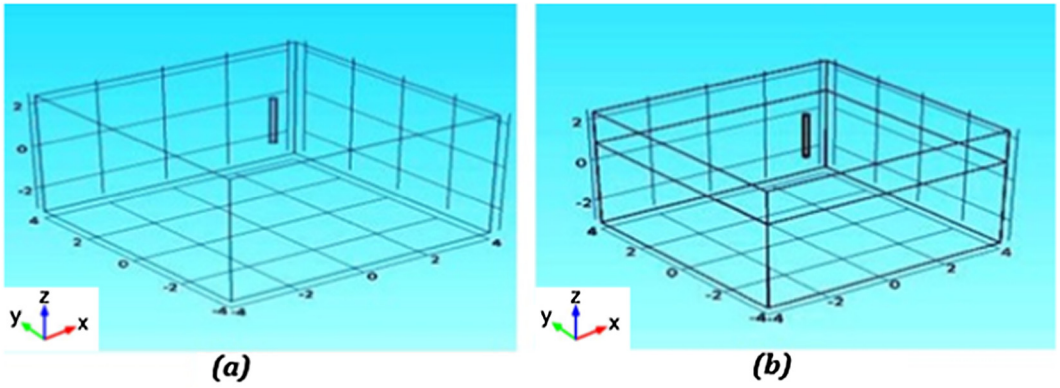

Fig. 7i. A schematic diagram of the 3D problem space for simulation of one vertical driven rod buried in: (a) one layer earth model, (b) two layers earth model.

electrodes. In addition, a Neumann boundary condition $\partial\varnothing/\partial n = 0$ at each cubic edge; while, n is the direction of the normal vector for each cubic face. For an isotropic resistivity (two-layer earth model), The electric potential satisfies the above boundary conditions as well as the boundary conditions given by Eq. (15), see Fig. 8.

4. Numerical results and discussions

4.1. Electric potential

Figs. 9a and 9b, describe the variation of the potential distribution along z-axis from the electrode surface to the ground surface

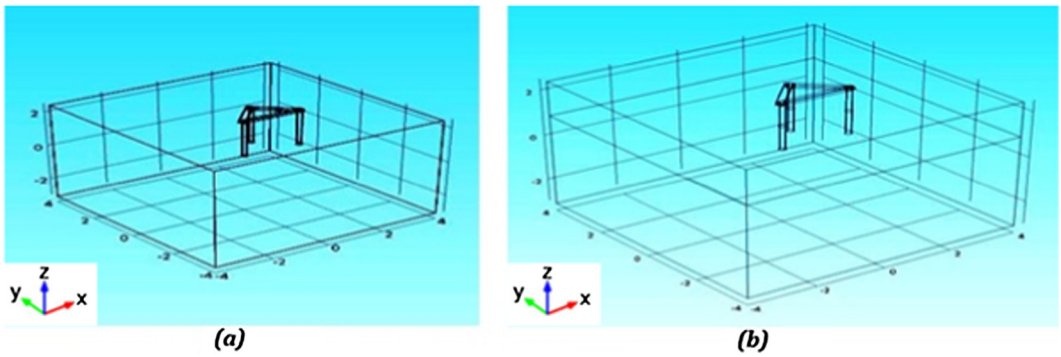

Fig. 7ii. A schematic diagram of the 3D problem space for simulation of three vertical driven rods buried in: (a) one layer earth model, (b) two layers earth model.

Table 1
Mesh statics and analysis condition for suggested model.

	Single driven rod		Three driven rods	
	One layer earth model	Two layers earth model	One layer earth model	Two layers earth model
Minimum element quality	0.2023	0.1569	6.314 E7	6.314 E7
Tetrahedral elements	14,883	14,017	91,367	90,828
Triangular elements	1476	1808	13,743	14,363
Edge elements	176	220	1560	1626
Vertex elements	16	24	106	122

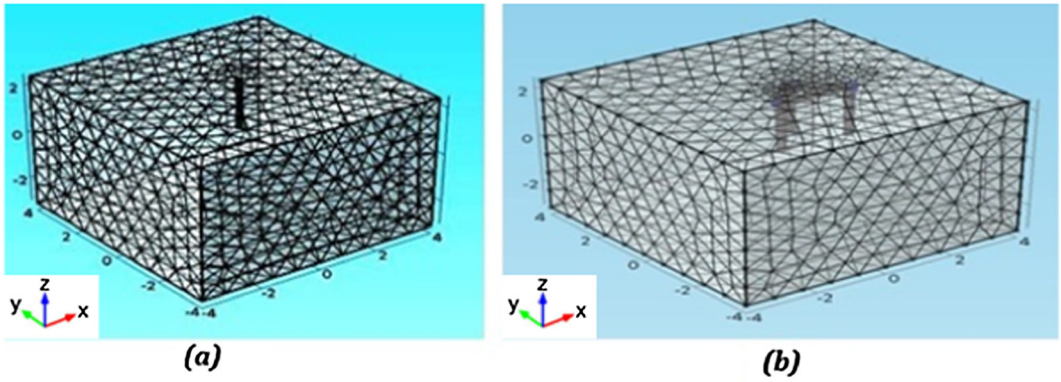

Fig. 7iii. Finite element discretization results for the 3D problem space (a) one vertical driven rod, (b) three vertical driven rods.

Table 2
Typical resistivity for different types of earth soil.

Type of soil	Typical resistivity $\rho(\Omega.m)$
Ashes of cinders	6–70
Clay (Damp)	14–30
Clay (Dry/Compacted)	100–200
Granite	2000–3000
Limestone	1000–5000
Loam (Humus)	200–400
Loam (with Sand and Gravel)	30–50
Loam (with some stones)	100–300
Loam (with stones and poor vegetation)	200–350
Marshy soils	300–400
Mountain rocks (with little soil)	5–40
Mountain soil (Damp peat over rock base)	1000–5000
Mountain soil (Over Rock Base)	150–300
Salt Pans	300–1000
Sand (Below Water Table)	6–70
Sand (Damp)	60–130
Sand (Dry)	1000–5000
Sand (Leached)	1000–5000
Sandstone	120–7000
Shales	100–160

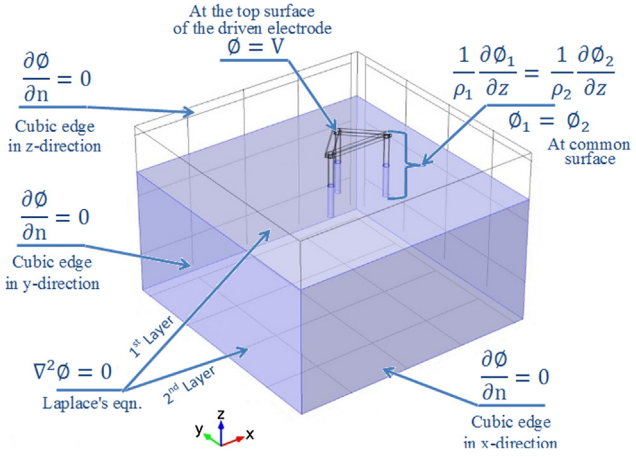

Fig. 8. A schematic diagram of the 3D problem for numerical solution of the electrical potential $\varnothing$.

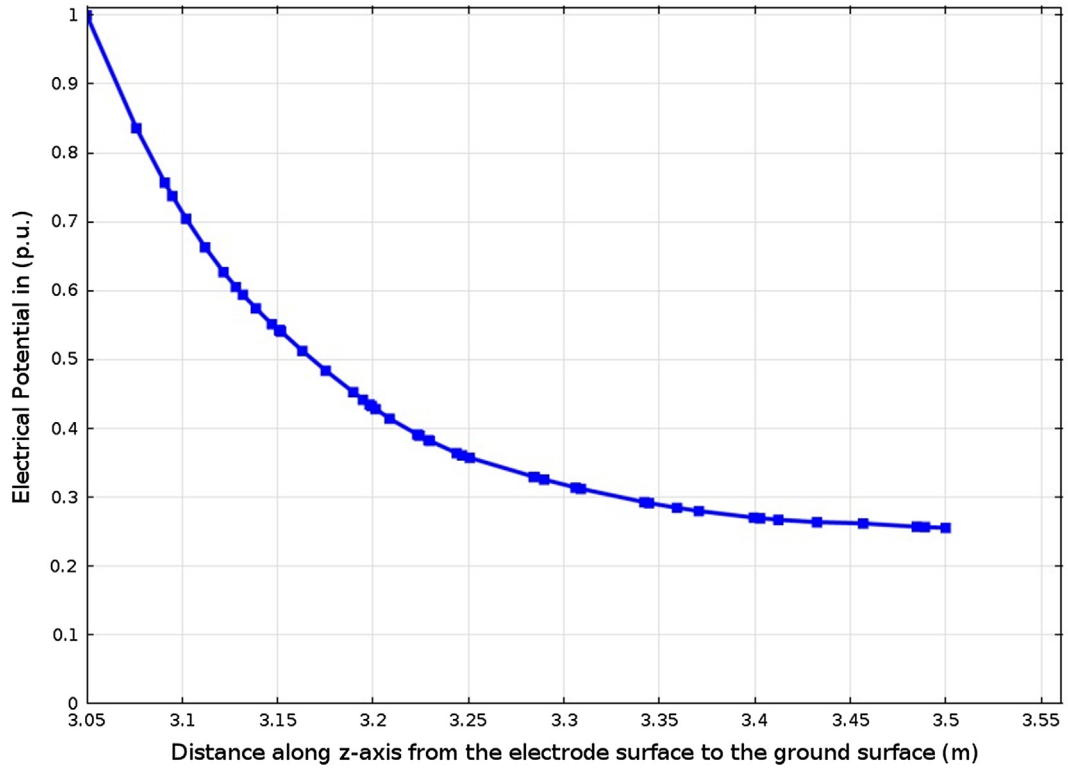

Fig. 9a. Electric potential distribution for one rod – One layer earth model in *p.u.* along z-axis from the electrode surface to the ground surface.

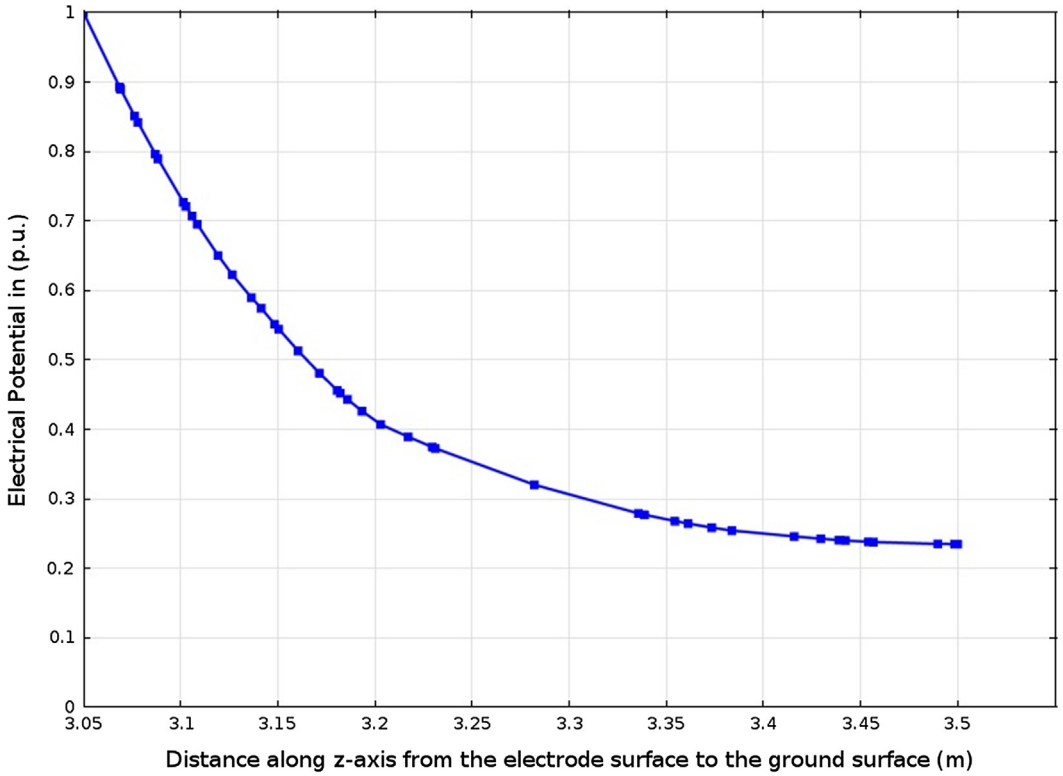

Fig. 9b. Electric potential distribution for one rod – Two layers earth model in *p.u.* along z-axis from the electrode surface to the ground surface.

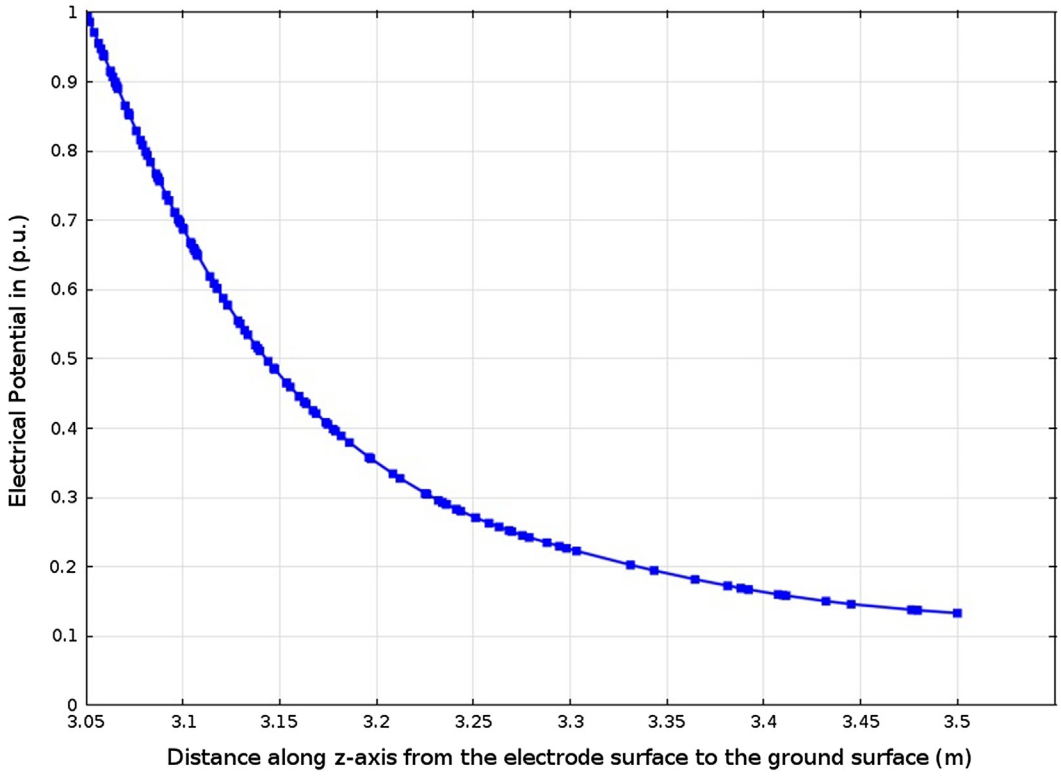

Fig. 9c. Electric potential distribution for three rods – One layer earth model in *p.u.* along z-axis from the electrode surface to the ground surface.

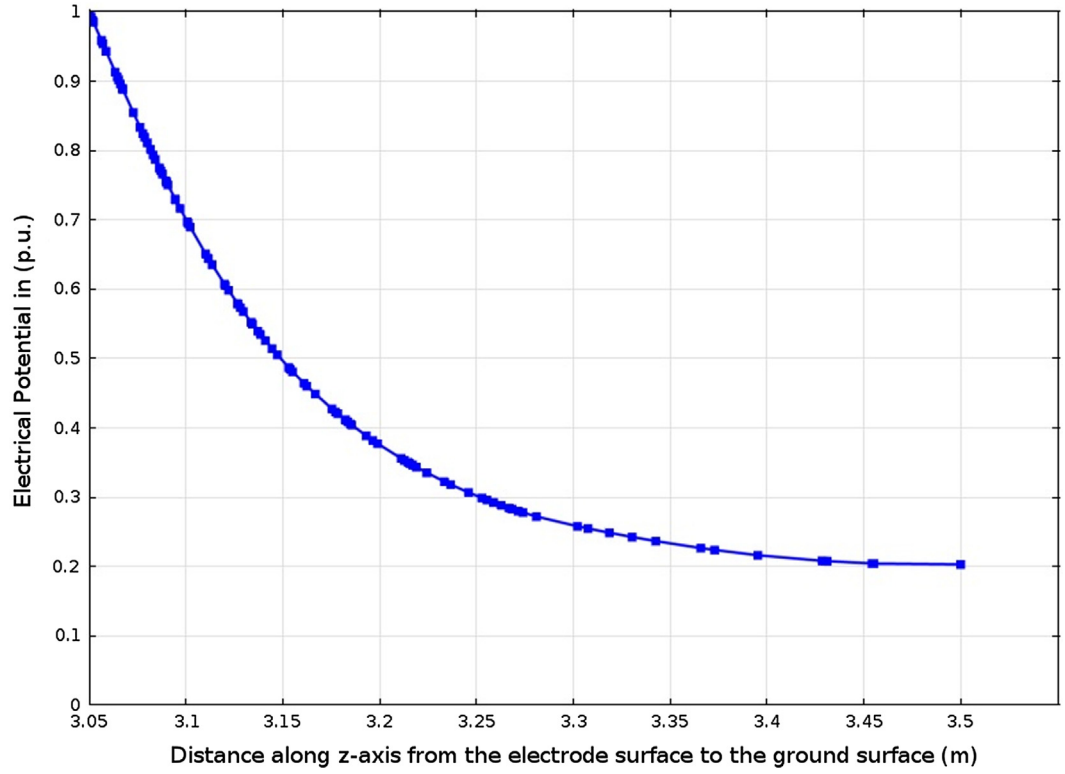

Fig. 9d. Electric potential distribution for three rods – Two layers earth model in *p.u.* along z-axis from the electrode surface to the ground surface.

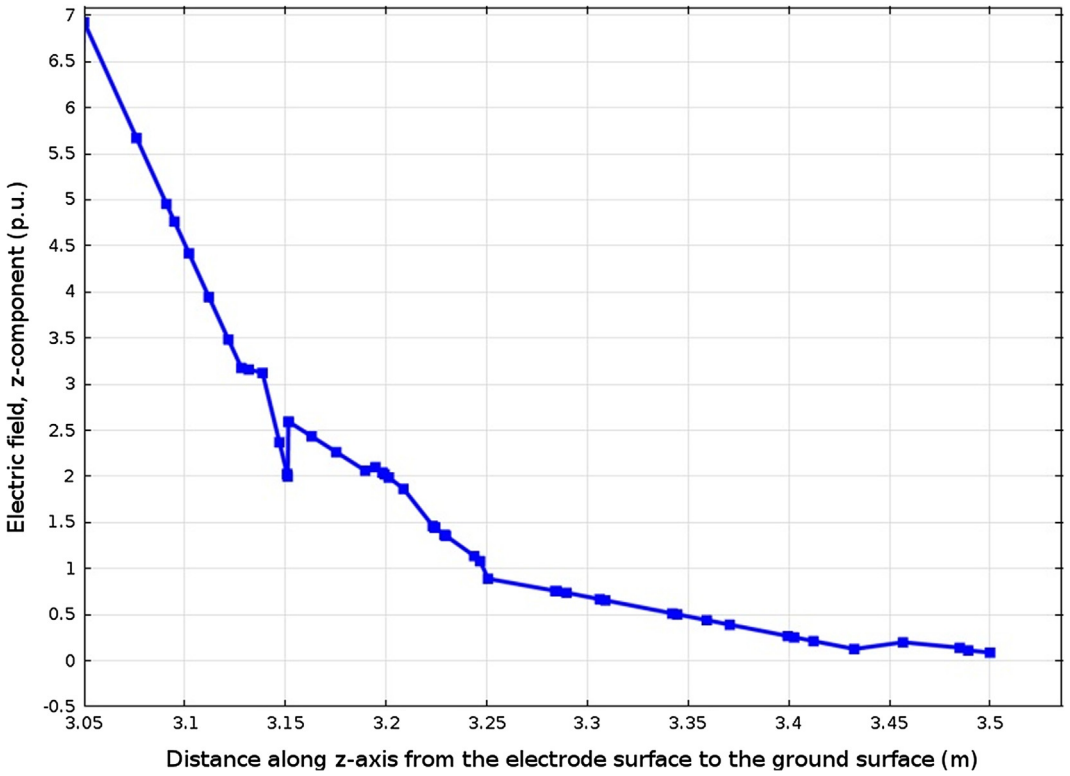

Fig. 10a. Electric field distribution for one rod-one layer earth model along z-axis from the electrode surface to the ground surface.

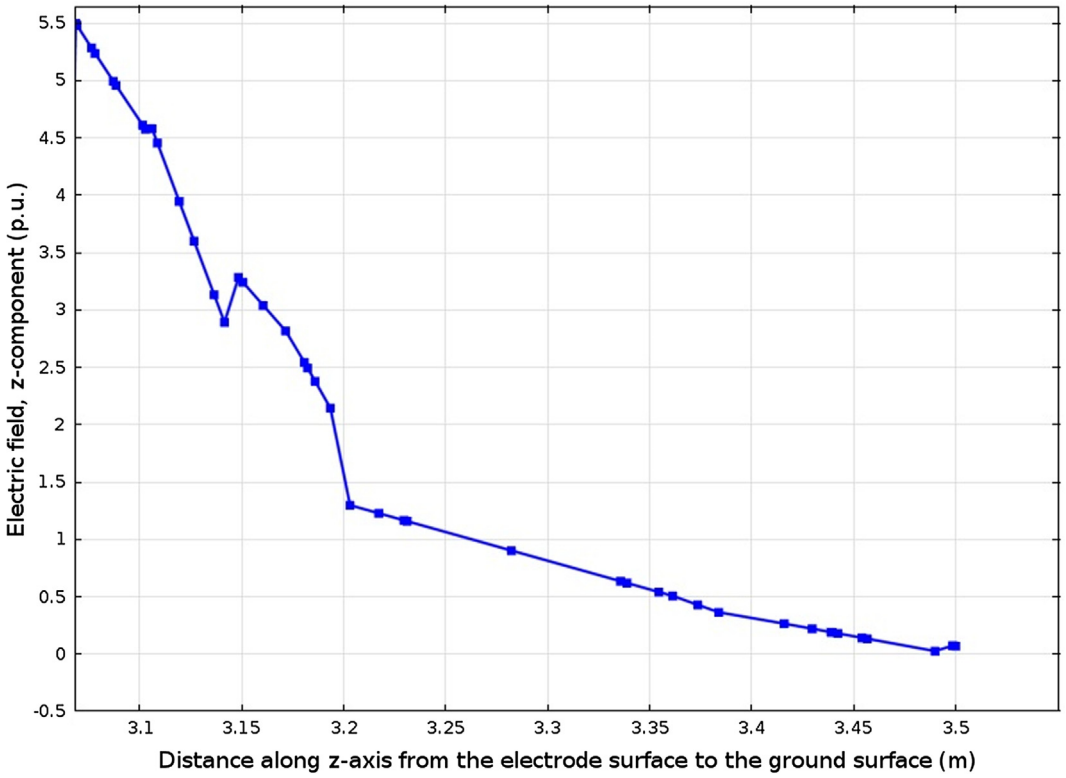

Fig. 10b. Electric field distribution for one rod-two layers earth model along z-axis from the electrode surface to the ground surface.

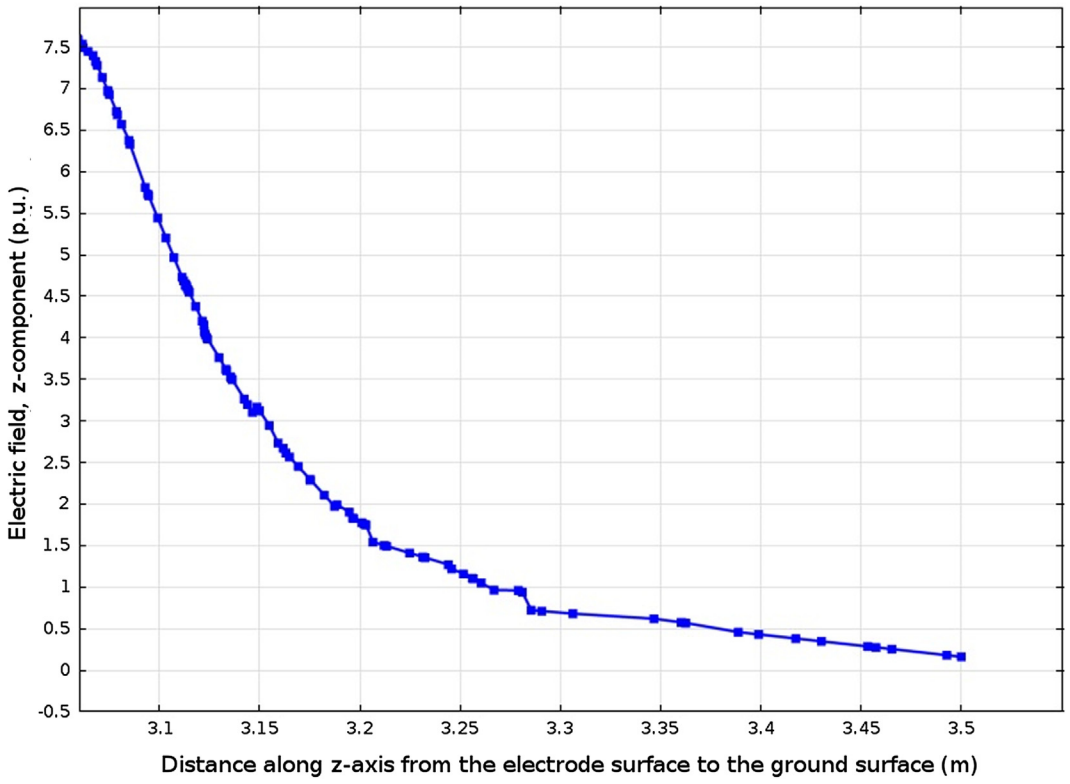

Fig. 10c. Electric field distribution for three rods-one layer earth model along z-axis from the electrode surface to the ground surface.

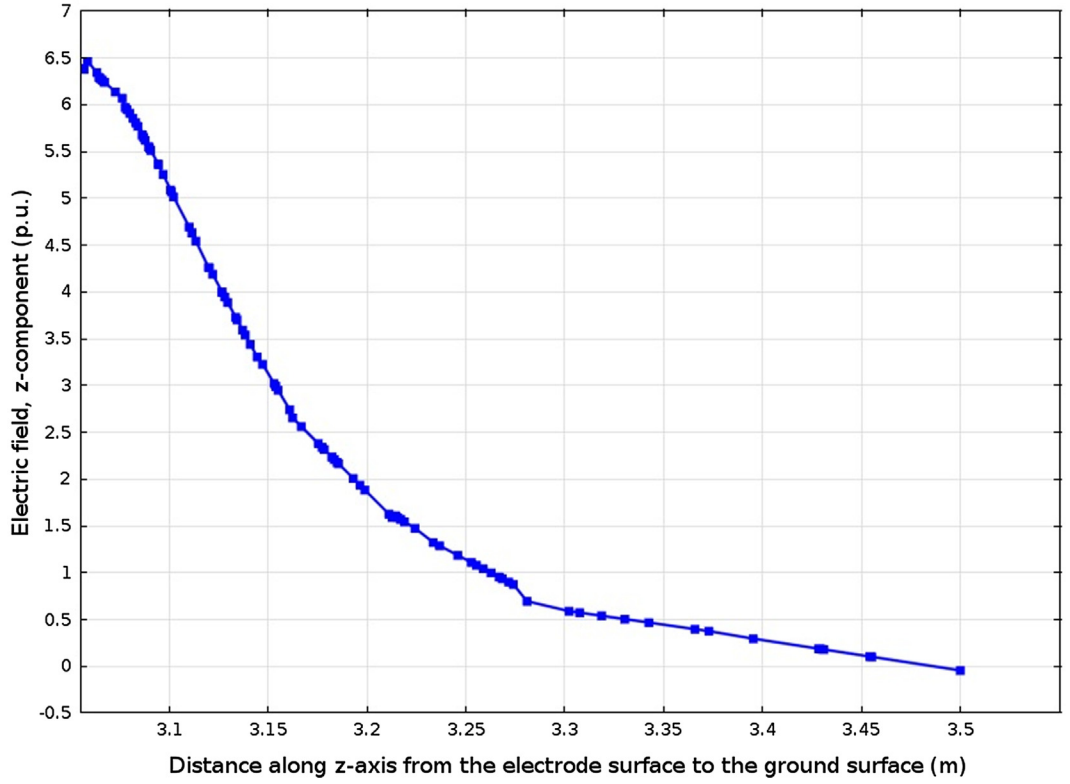

Fig. 10d. Electric field distribution for three rods-two layers earth model along z-axis from the electrode surface to the ground surface.

for one rod in the case of one and two layers earth model respectively. From these two figures, the value of the earth surface potential obtained from the potential in z direction is nearly constant at 0.25$p.u.$ of the value of the applied voltage.

While Figs. 9c and 9d, give the distribution of the potential along z-axis from the electrode surface to the ground surface for three rods in the case of one and two layers earth model respectively. These figures give the explanation of why the three driven rods are commonly used, It is clear that the value of the earth surface potential decreases to 0.14$p.u.$ in case of one layer earth model and to 0.2$p.u.$ in the case of two layers earth model. This is due to the reduction in the ground resistance in case of three rods. Also in this case the variations in soil resistivity have considerable influence on the ground resistance and earth surface potential.

4.2. The electric field distribution along the driven electrode

Figs. 10a–10d describe the electric field distribution along the $z-axis$ of the driven vertical rod surface in the case of one rod-one layer, one rod-two layers, three rods-one layer and three rods-two layers earth models respectively. From these Figures, the high disturbance of the electric field is near to the earth surface (about 0.5m below the ground surface) at the top surface of the driven vertical rod, (about 7$p.u.$ in case of one rod – One layer and about 5.5$p.u.$ in case of one rod – Two layers), also (about 7.5$p.u.$ in case of three rods – One layer and about 6.5$p.u.$ in case of three rods – Two layers). But this disturbance is eliminated and reached zero at the ground surface. These results agree will with results given by [2] and the IEEE standard [32].

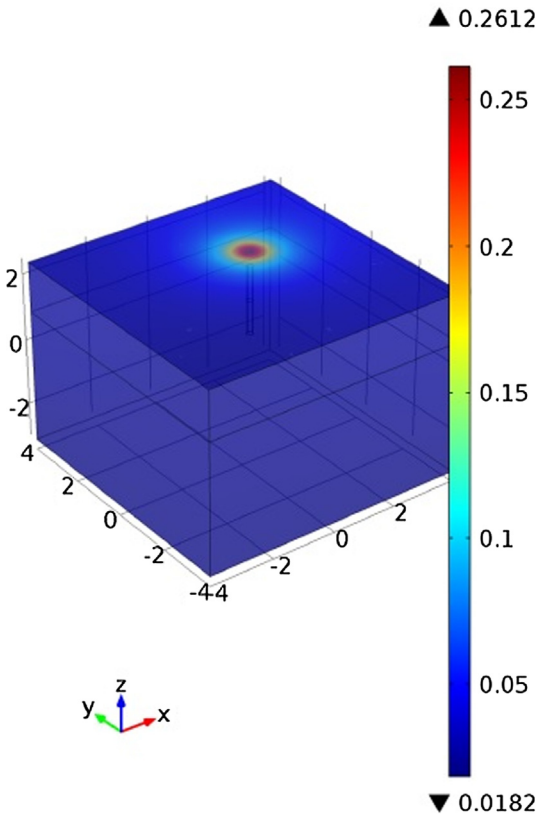

Fig. 11b. Ground potential rise simulation along the ground surface in case of one rod-two layers earth model.

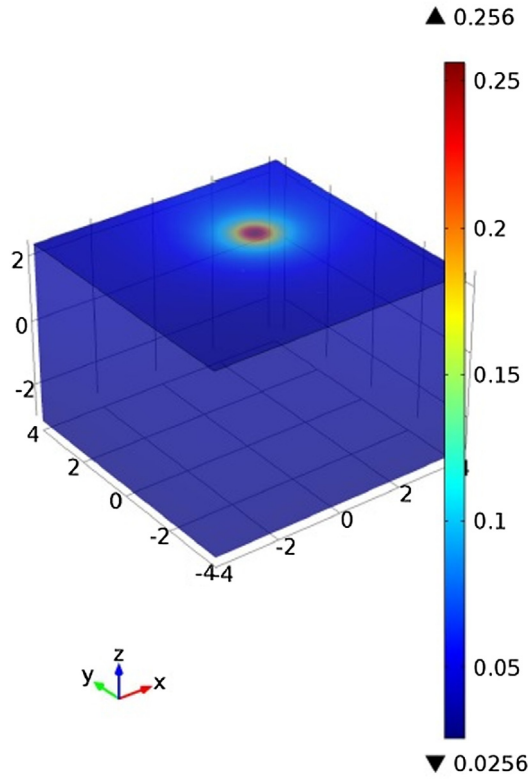

Fig. 11a. Ground potential rise simulation along the ground surface in case of one rod-one layer earth model.

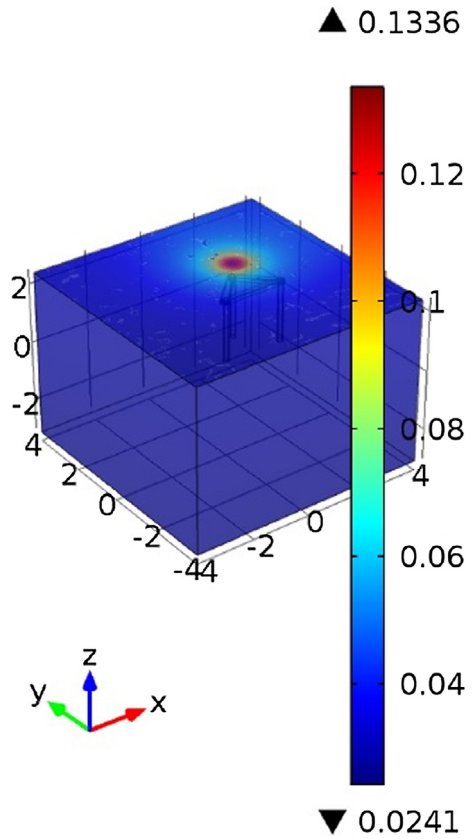

Fig. 11c. Ground potential rise simulation along the ground surface in case of three rods-one layer earth model.

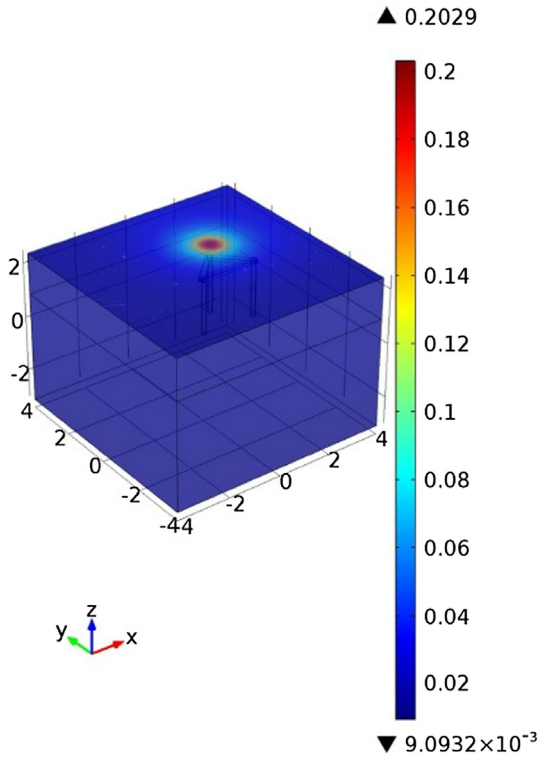

Fig. 11d. Ground potential rise simulation along the ground surface in case of three rods-two layers earth model.

4.3. The ground potential rise (GPR) simulation along the ground surface

Figs. 11a–11d describe the simulation of the GPR at the ground surface in the region around the buried driven rod in the case of one rod-one layer, one rod-two layers, three rods-one layer and three rods-two layers earth models respectively. It is clear that the value of the GPR in the case of one rod – One layer varies from 0.0256 to 0.256 *p.u*., and varies from 0.0182 to 0.2612 *p.u*. in case of one rod – Two layers which is higher than the case of three rods, the GPR in the case of three rods – One layer varies from 0.0241 to 0.1336 *p.u*., and varies from 9.09×10^{-3} to 0.2029 *p.u*. in case of three rods – Two layers, so the GPR is reduced in case of three-driven rods to about the half value in case of one driven rod. This can explain the benefits of three-driven rods and homogenous model in case of safety of the earthing systems. Also from these figures, it is also obvious that the disturbance in the GPR is increased in case of anisotropic resistivity (two-layer earth model).

5. The Comparison with available experimental data

In order to enhance the influence of the electric fields on the complex earthing system and to estimate the GPR, a case study of earthing system for silos region in Egypt was investigated (see Figs. 12a–12c). The silos earthing system was subjected to an applied voltage of 5*kV* for each of one rod stand alone and three connected rod considering the case of one layer earthing model with clay RDP (relative dielectric permittivity) of 15. The dimension of the silos earthing rods and distance between them are in

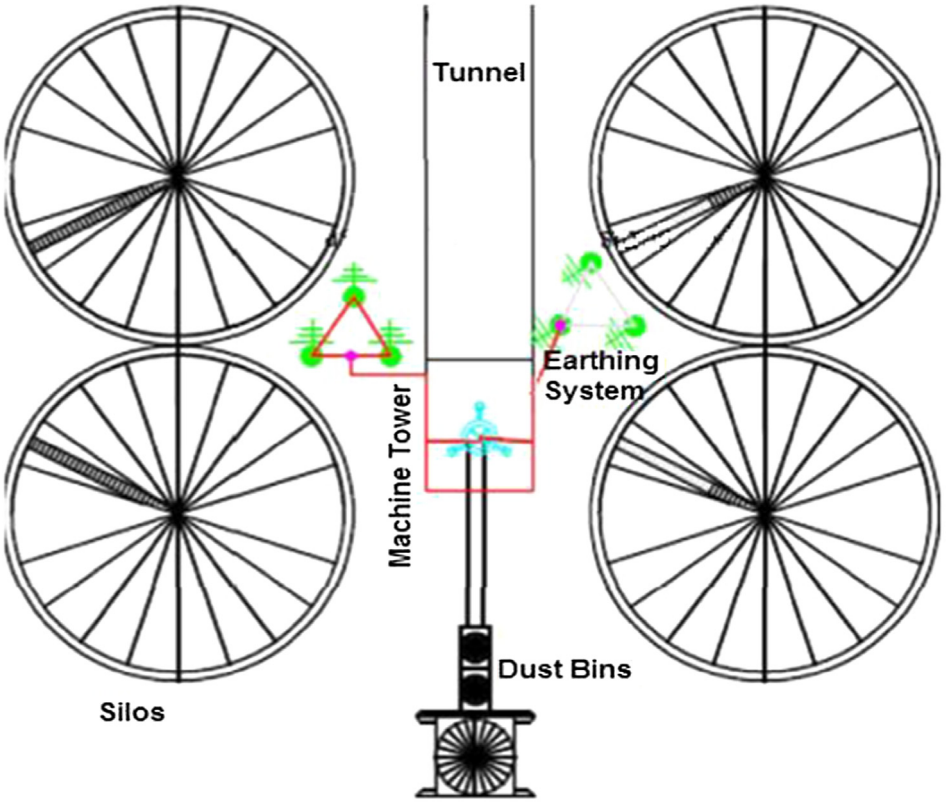

Fig. 12a. Schematic diagram of earthing system for silos region (case study in Egypt).

Fig. 12b. The three manholes for the three earth electrodes of silos region.

Fig. 12c. The details of one manhole containing one earth electrode.

Table 3
Comparison with experimental results for one layer model.

	Ground potential rise in (*p.u.*) "5 *kV* base"	
	Single driven rod	Three driven rods
Simulation result	0.25	0.14
Experimental result	0.235	0.1368

Table 4
Comparison with others experimental results for three driven rods one layer model.

	Proposed model	Ref. [33]	Ref. [34]	Ref. [35]
GPR in (p.u.)	0.14	0.1476	0.16	0.15

accordance with the simulation model. The measured values of GPR from the silos earthing system are tabulated in Table 3, assuming that $5kV = 1p.u.$

Therefore, the numerical computation is in a good concordance with the experimental one given by [33–35] (as shown in Table 4), which describes the GPR along the vertical axis of the electrode surface. This agreement gives a good indication about the calculation of the electric field distribution at the ground surface and the GPR at the ground surface from this simulation.

6. Future considerations

Usually, the electric field effects are accompanied by thermal effects due to Joule's heating. This coupled effect can be modeled and simulated by using the commercial software ANSYS Fluent. It is a finite volume computational fluid dynamics software that can model magnetic, electric, fluid flow, and thermal effects coupled with each other. Unstructured grid of 1,398,505 cells was created in this domain to simulate both effect of the electric field and the thermal effects. Transient simulation was conducted to study the time effect of heat propagation in the copper parts with time. Initial simulation results showed that the temperature of the connecting rods can reach $454K$ with applied voltage of $5kV$ after a time of 50 microseconds. This is applied in the three rods case in Loam type ground, see Fig. 13. This shows that heat transfer effects are very important to validate security of the earthing that are used in different application. Also, it was found that the high temperatures are concentrated at the sharp edges of the connectors.

To study the temporal variation of temperature under the applied voltage, the maximum copper temperature was plotted with simulation time as shown in Fig. 14. It was found that the variation of the maximum temperature increases linearly with time. The maximum temperature captured after a period of 100 microsecond simulation was $607K$.

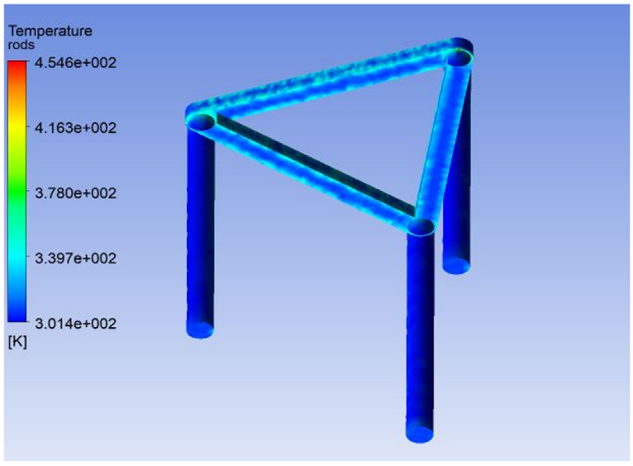

Fig. 13. The simulation of the thermal effect.

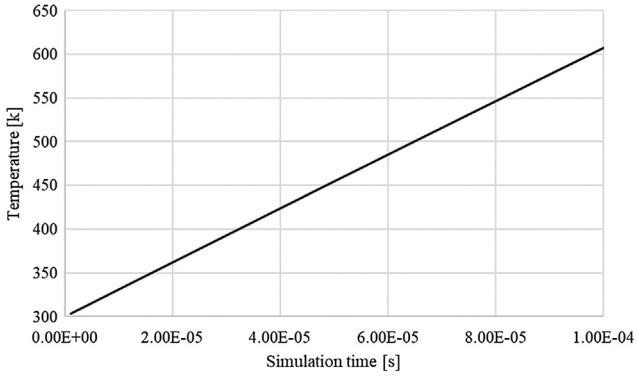

Fig. 14. Temporal variation of the maximum temperature of copper rods and connector under 5 *kV* applied voltage.

7. Conclusions

Various cases of GPR and the electric field distribution in two cases of isotropic and anisotropic resistivity and two models of one driven rod and three driven rods have been analyzed. A new simulation model for potential and electric field is presented. This model is certified by using finite element method (FEM) with the principles of partial differential equations (PDE). This simulation is a three-dimensional (3D) problem space; the software computer program which is used to build this model is COMSOL Multiphysics program. The simulation model gives the values of GPR and the electric field at the ground surface, also the distribution of the potential and vertical field along the driven vertical rod. The results showed that the three-rods earthing system is much better than one rod earthing system with respect to GPR and the value of the electric field at the ground surface, the results also demonstrated that the type of the soil is very important for the field distribution along the ground surface.

After accurate simulation, the following points can be illustrated for the studied model and the values used:

1. The more the vertical driven rods number increase, the more the value of the surface potential at the ground surface decrease, which means that it is more safety to increase the numbers of vertical driven rods in the earthing system as cleared that the three rods earthing system is much better than one rod.
2. The benefits of connecting the vertical driven rods together, which resulting in reducing the value of surface potential distribution due to the decreasing of the whole grounding system resistance
3. The maximum value of the GPR for one driven vertical rod is $0.256p.u.$ for one layer and $0.2612p.u.$ for two layers
4. The maximum value of the GPR for three driven vertical rods is $0.1336p.u.$ or one layer and $0.2029p.u.$ for two layers
5. The GPR is increased in case of anisotropic resistivity (two-layer earth model)
6. The three rods earthing system is much better than one rod.
7. The high value of the electric field is at the top surface of the driven vertical rod, which reaches about $7p.u.$ in the horizontal direction inside the soil at the top surface of the driven electrode, which agree with results given by [2,32].
8. The electric field at the ground surface above an earthing system directly is less than $0.07p.u.$ these values should be kept in a range which is less than $1p.u.$ according to IEEE Safety Guide [32].
9. FEM is adopted for electric field simulation in case of three-dimension field problem.
10. The simulated temperature of the connecting rods can reach $454K$ with applied voltage of $5kV$ after a time of 50 microseconds.

Appendix A

One-layer earth model:

The expression of the potential satisfies Laplace equation,

$$\begin{aligned} \nabla^2 \varnothing &= 0.0 \\ \tfrac{\partial^2 \varnothing}{\partial r^2} + \tfrac{1}{r}\tfrac{\partial \varnothing}{\partial r} + \tfrac{\partial^2 \varnothing}{\partial z^2} &= 0.0 \end{aligned} \tag{a-1}$$

By applying the method of variables separation [21],

$$\left.\begin{aligned} \varnothing(r,z) &= R(r)Z(z) \\ \tfrac{\partial \varnothing}{\partial r} &= \tfrac{\partial R}{\partial r} Z \\ \tfrac{\partial^2 \varnothing}{\partial r^2} &= Z\tfrac{\partial^2 R}{\partial r^2} \\ \tfrac{\partial^2 \varnothing}{\partial z^2} &= R\tfrac{\partial^2 Z}{\partial z^2} \end{aligned}\right\} \tag{a-2}$$

From Eq. (a-2) substitute into Eq. (a-1)

$$Z\frac{\partial^2 R}{\partial r^2} + \frac{1}{r}\frac{\partial R}{\partial r}Z + R\frac{\partial^2 Z}{\partial z^2} = 0.0$$

Divided by RZ

$$\frac{1}{R}\frac{\partial^2 R}{\partial r^2} + \frac{1}{Rr}\frac{\partial R}{\partial r} + \frac{1}{Z}\frac{\partial^2 Z}{\partial z^2} = 0.0$$

$$\frac{1}{R}\frac{\partial^2 R}{\partial r^2} + \frac{1}{Rr}\frac{\partial R}{\partial r} = -\frac{1}{Z}\frac{\partial^2 Z}{\partial z^2} = m^2 \tag{a-3}$$

The first part of Eq. (a-3) is

$$\frac{\partial^2 Z}{\partial z^2} + m^2 Z = 0.0$$

The solution of the first part is $\sin(mz)$and $\cos(mz)$.

The second part of Eq. (a-3) is

$$\frac{\partial^2 R}{\partial r^2} + \frac{1}{r}\frac{\partial R}{\partial r} - m^2 R = 0.0$$

The solution of the second part is $J_o(mr)$ and $K_o(mr)$, where, $J_o(mr)$ and $K_o(mr)$ are respectively the modified Bessel's function of first and second kind with order of zero.

Since the potential is independent of z sign, therefore $\cos(mz)$ will be the proper potential function, so the potential is given by,

$$\varnothing = \int_0^\infty A(m) J_o(mr)\cos(mz)dm \tag{a-4}$$

where, $A(m)$ is arbitrary Kernel function.

For this problem, the Weber Lipschitz's integral can be written as,

$$\begin{aligned} A(m) &= \tfrac{\rho I}{2\pi} \\ \varnothing &= \tfrac{\rho I}{2\pi}\int_0^\infty J_o(mr)\cos(mz)dm \end{aligned} \tag{a-5}$$

Appendix B

Two-layers earth model:

The expression of the potential satisfies Laplace equation,

$$\begin{aligned} \nabla^2 \varnothing &= 0.0 \\ \tfrac{\partial^2 \varnothing}{\partial r^2} + \tfrac{1}{r}\tfrac{\partial \varnothing}{\partial r} + \tfrac{\partial^2 \varnothing}{\partial z^2} &= 0.0 \end{aligned} \tag{b-1}$$

The solution of the first part of Eq. (a-3) is $\sin(mz)$ and $\cos(mz)$and the general solution of the Eq. from (a-4) considering the $\sin(mz)$ and $\cos(mz)$ term is

$$\varnothing = \int_0^\infty [A(m)\cos(mz) + B(m)\sin(mz)]J_o(mr)dm \tag{b-2}$$

$$\varnothing = \int_0^\infty [A(m)e^{-mz} + B(m)e^{mz}]J_o(mr)dm \tag{b-3}$$

For surface geophysics, the potential at the earth surface at distance x, see Fig. 4, due to a current source on the surface as given from Eq. (7) of an N-layered earth is

$$\varnothing_o = \frac{\rho I}{2\pi}\int_0^\infty e^{-m|z|}J_o(mx)dm \tag{b-4}$$

From Eq. (8), the source potential can be written as

$$\varnothing_o = \frac{\rho I}{2\pi}\frac{1}{\sqrt{x^2+z^2}}$$

The potentials in the different layers can, therefore, be written as follows,

$$\varnothing_1 = \varnothing_o + \varnothing_1^{'}$$

$$\varnothing_2 = \varnothing_o + \varnothing_2^{'}$$

where, $\varnothing_1^{'}$ and $\varnothing_2^{'}$ are the perturbation potentials in different media.

Potential at the ith media can be written as

$$\varnothing_i = \frac{\rho_i I}{2\pi}\frac{1}{\sqrt{x^2+z^2}} + \int_0^\infty [A_i(m)e^{-mz} + B_i(m)e^{mz}]J_o(mx)dm \tag{B5}$$

where, A_i and B_i are the arbitrary constants, these constants can be determined from the boundary conditions. At the earth- air boundary surface, the current density cannot across the air, therefore,

$$\frac{1}{\rho_i}\frac{\partial\varnothing_i}{\partial z} = 0 \; at \; z = 0$$

$$\left(\frac{\partial\varnothing}{\partial z}\right)_{z=0} = \left\{\frac{\rho_i I z}{2\pi\sqrt{x^2+z^2}} + \int_0^\infty m(-A_i e^{-mz} + B_i e^{mz})J_o(mx)dm\right\}_{z=0} = 0$$

$$\left(\frac{\partial\varnothing}{\partial z}\right)_{z=0} = \int_0^\infty m(B_i - A_i)J_o(mx)dm = 0$$

$$B_i = A_i$$

Therefore, the expression for potential in the first medium is

$$\varnothing_1 = \varnothing_o + \int_0^\infty A_1(m)(e^{-mz} + e^{mz})J_o(mx)dm \tag{b-6}$$

The value of $A_1(m)$ can be determined using the initial boundary condition.

References

[1] A. Swetapadma, A. Yadav, A hybrid method for fault location estimation in a fixed series compensated lines, Measurement 123 (July 2018) 8–18.
[2] M. Talaat, M.A. Farahat, M. Osman, Assessment of earthing system location for wind turbines using finite element method, Renew. Energy 93 (2016) 412–423.
[3] H. Bell, Protection of A.C Systems, J. IEE 6 (70) (1960) 571–575.
[4] C. Mazzetti, G.M. Veca, Impulse behaviour of ground electrodes, IEEE Trans Power Apparat. Syst. PAS 102 (9) (1983) 3148–3158.
[5] S. Farag, T.C. Cheng, D. Penn, Ground terminations of lightning protective systems, IEEE Trans. Dielectr. Electr. Insul. 5 (6) (1998) 869–877.
[6] E.M. Bazelyan, YuP. Raizer, N.L. Aleksandrov, Corona initiated from grounded objects under thunderstorm conditions and its influence on lightning attachment, Plasma Sour. Sci. Technol. 17 (2) (2008).
[7] Reinhold Rüdenberg, Transient Performance of Electric Power System, Phenomena in Lumped Networks, first edition., McGraw-Hill Book Company, Inc., 1950, 328-336, and pp. 383-387 Printed in USA.
[8] H. Motoyama, Electromagnetic transient response of buried bare wire and ground grid, IEEE Trans. Power Deliv. 22 (3) (2007) 1673–1679.
[9] A. El Mghairbi, M. Ahmeda, N. Harid, H. Griffiths, A. Haddad, Technique to increase the effective length of practical earth electrodes: Simulation and field test results, Electr. Power Syst. Res. 94 (2013) 99–105.
[10] M. Talaat, Calculation of electrostatically induced field in humans subjected to high voltage transmission lines, Electr. Power Syst. Res. 108 (2014) 124–133.
[11] A. Ametani, T. Chikaraaa, H. Moriib, T. Kubob, Impedance characteristics of grounding electrodes on earth surface, Electr. Power Syst. Res. 85 (2012) 38–43.
[12] Takehiko Takahashi, Taro Kawase, Calculation of earth resistance for a deep-driven rod in a multi-layer earth structure, IEEE Trans. Power Deliv. 6 (2) (1991) 608–614.
[13] Li-Hsiung Chen, Jiann-Fuh Chen, Tsorng-Juu Liang, Wen-I Wang, Calculation of ground resistance and step voltage for buried ground rod with insulation lead, Electr. Power Syst. Res. 78 (2008) 995–1007.
[14] M. Talaat, Electrostatic field calculation in air gaps with a transverse layer of dielectric barrier, J. Electrostat. 72 (5) (2014) 422–427.
[15] Jinxi Ma, Farid Paul Dawalibi, Computerized analysis of grounding plates in multilayer soils, IEEE Trans. Power Deliv. 24 (2) (2009) 650–655.
[16] Jovan Nahman, Ivica Paunovic, Mesh voltages at earthing grids buried in multi-layer soil, Electr. Power Syst. Res. 80 (2010) 556–561.
[17] J.A. Güemes, F.E. Hernando, Method for calculating the ground resistance of grounding grids using FEM, IEEE Trans. Power Deliv. 19 (2) (2004) 595–600.
[18] Farid Dawalii and Dinkar Mukhedkar, "Optimum design of substation grounding in a two layer earth structure Part I - Analytical study", in IEEE Transactions on Power Apparatus and Systems, Vol. PAS-94, No. 2, pp. 252–261, 1975.
[19] Enrique Bendito, Ángeles Carmona, Andrés M. Encinas, M. José Jiménez, The extremal charges method in grounding grid design, IEEE Trans. Power Deliv. 19 (1) (2004) 118–123.
[20] M.K. AbdElrahman, An advanced technique for earthing system analysis, IEEE Trans. Power Deliv. 28 (1) (2013) 268–275.
[21] Kalyan Kumar Roy, Potential Theory in Applied Geophysics, Springer-Verlag, Berlin Heidelberg, New York, 2008, pp. 211–223.
[22] E.D. Sunde, Earth Conduction Effects in Transmission line Systems, Dover Publications Inc., 1968.
[23] COMSOL AC/DC Module User's Guide, COMSOL 4.3.
[24] M. Talaat and N. H. Mostafa,"Use of finite element method for the numerical analysis of eddy current brake", IEEE 15th International Workshop on Research and Education in Mechatronics, REM 2014, pp. 1–7, 2014.
[25] Marcos S. Vieira, Jorge M. Janiszewski, Propagation of lightning electromagnetic fields in the presence of buildings, Electr. Power Syst. Res. 118 (2015) 101–109.
[26] Mladen Trlep, Anton Hamler, Bozidar Hribernik, The analysis of complex grounding systems by FEM, IEEE Trans. Magn. 34 (5) (1998) 2521–2524.
[27] M. Talaat, A. El-Zein, A numerical model of streamlines in coplanar electrodes induced by non-uniform electric field, J. Electrostat. 71 (3) (2013) 312–318.
[28] M. Talaat, A. El-Zein, M. Amin, Electric field simulation for uniform and FGM cone type spacer with adhering spherical conducting particle in GIS, IEEE Trans. Dielectr. Electr. Insul. 25 (1) (February 2018) 339–351.
[29] M. Talaat, A. El-Zein, M. Amin, Developed optimization technique used for the distribution of u-shaped permittivity for cone type spacer in GIS, Electr. Power Syst. Res. (2018), https://doi.org/10.1016/j.epsr.2017.07.002.
[30] M. Talaat, M.A. Farahat, Taghreed Said, Numerical investigation of the optimal characteristics of a transverse layer of dielectric barrier in a non-uniform electric field, J. Phys. Chem. Solids 121 (2018) 27–35.
[31] M. Talaat, H.M.B. Metwally, I. Arafa, Experimental and simulation study of wireless power transfer using resonators with coupled electric fields, IEEE Transactions on Plasma Science 46 (7) (2018).
[32] IEEE Guide for safety in AC substation grounding, IEEE Std.80-2000.
[33] N. MohamadNor, M. Trlep, S. Abdullah, R. Rajab, Investigations of earthing systems under steady-state and transients with FEM and experimental work, Electr. Power Energy Syst. 44 (2013) 758–763.
[34] Silverio Visacro, Miguel B. Guimaraes, Listz S. Araujo, Experimental impulse response of grounding grids, Electr. Power Syst. Res. 94 (2013) 92–98.
[35] J. Nahman and D. Jelovac, "High-voltage/medium(low)-voltage substation earthing systems", IEE Proceedings C Generation, Transmission and Distribution,Vol. 134, No. 1, pp. 75–80, 1987.